Chapter 3

Predictive theory for experiments on microbes on the energetic brink

Many cells—including microbes that power our planet's carbon cycle, nurture our agriculture, or devastate our human lungs—orchestrate their physiology under severe bioenergetic limitations. Such metabolically-constrained cells are not just slowed-down versions of the fast-growing cells well studied by most laboratory experiments. Instead, these cells on the metabolic brink are completely remodeled organisms and must follow distinct quantitative principles, tradeoffs, and strategies to survive [1, 2]. These extraordinary physiological states at energetic extremes give unique opportunities to identify critical consequences of the nonequilibrium energy expenditures that distinguish life from nonliving matter.

Careful experimental studies probing the physiology of energy-limited microbes are rare but reveal quantitative regularities for canonical perturbations like carbon deprivation [3]. On the other hand, there is far more to environmental challenges than carbon deprivation. In this chapter, we strive to make forceful links between experimentally tractable observables and the often quite different "theorist variables" actually underlying

energy-limited cells as dynamical systems. Our aim is to move slightly away from philosophizing grandly with cartoons and verbal statements. Here we seek to ask, what are the precise consequences of different mathematical and physiological universes on a spectrum of real measurable experimental quantities? Further, how can we learn from the inverse problem of how macroscopic phenomenology of abundance constrains the metabolic states and operations maintained by cells? We are inspired by unprecedented measurements on total metabolism, and rich accompanying trajectories of cell counts, by investigators in the laboratory of Dianne Newman and colleagues.

This chapter takes its journey in three parts. First, in §3.1, we ask about the phenomenology of death. Why do populations of dying cells drop so differently under oxygen starvation compared to carbon starvation? We give a simple quantitative origin story for these big macroscopic differences. Second, in §3.2, we pose humble kinetic pictures for the particulars of real experiments culturing cells with electrodes, and analyze these models' consequences. We hope these different experimentally-testable consequences might help rigorously distinguish between models that otherwise seem competitively credible. Third, in §3.3, we analyze pilot experiments on *Pseudomonas* in varied salt conditions. Amid some rich phenomenology, this allows us to preliminarily estimate a valuable characteristic parameter specifying the changes in metabolic rate demanded of cells in greater environmental salt conditions. We quantitatively contrast this parameter in *Pseudomonas* with an anlog we infer from very separate data in *E. coli*, uncovering striking differences.

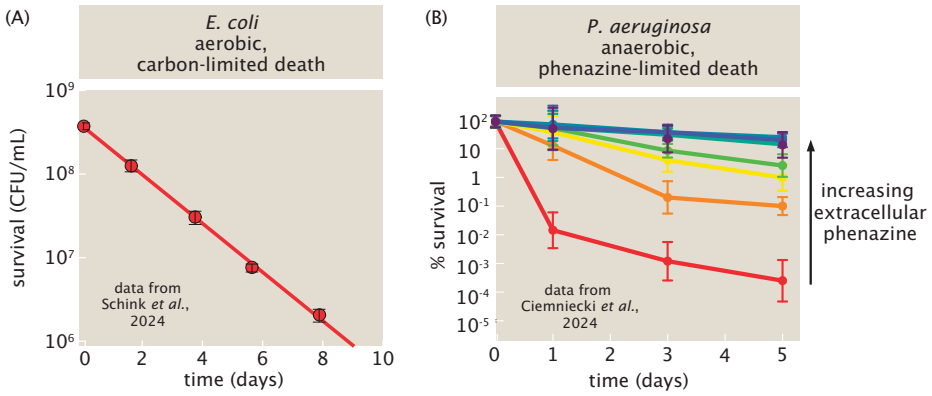

Figure 3.1: Empirical death curves for cells subjected to different deprivations. (A) *E. coli* cells deprived of carbon show a stereotyped death profile. (B) *P. aeruginosa* deprived of a terminal electron acceptor shows a markedly different death profile. Unlike the electron donor- (carbon-) limited growth case at left, the terminal electron acceptor case shows conspicuous changes to the per-capita death rate over time. Distinct color traces refer to different ambient concentrations of extracellular phenazine as a terminal electron acceptor. The carbon-limited data are from Schink *et al. Nat. Phys.* 2024 [4]; the phenazine-limited data are from Ciemniecki *et al.* 2024 [5].

3.1 Phenomenology of death differs under terminal e^- acceptor or donor deprivation

When starved of terminal electron acceptors, such as oxygen or phenazines, for example, cells die differently than when they are starved of electron donors such as carbon. This distinction manifests itself at a population level. As shown in Figure 3.1(A), when starved of carbon, viable cells often decline at constant exponential rates, showing linear declines in abundance measured on a log scale over time. In contrast, cells die at markedly time-varying rates when anaerobically starved of phenazine, making log abundance drop at slowing rates over time, as shown in Figure 3.1(B).

What physiology and dynamics of resource exchange with the environment account for these differences? Can these features further report on the underlying bioenergetic status of stressed cells, for example to eventually infer maintenance metabolic rates from population abundances alone (once calibrated by precise redox current measurements)? Towards these questions, here we formulate candidate models capturing the distinct

balances between cellular energy consumption and bioenergetic resource supply from the environment (or from other dying cells) underlying terminal electron acceptor or electron donor deprivation.

Our central contention for why these macroscopic phenomenologies of death differ when the electron donor is limiting, versus when the electron acceptor is limiting, is simply stated. When carbon is limiting, dying and lysing cells, which are made up of the very thing that is limiting the energetic state of the cells, can help feed and sustain the cells that remain alive. This dynamic is schematized in Figure 3.2(A), and is exactly the beautiful quantitative picture developed and quantitatively stress-tested by the experimental work of Schink, Gerland, Basan and coworkers for *E. coli* under carbon limitation [6, 7, 4]. In this picture, the energetic demand of an instantaneous abundance of cells is exactly balanced by a supply proportional to the current death rate, yielding the quantitative regularity of the per-capita death rate visible in survival curves like that in Figure 3.1(A). Specifically, if the limiting energy pool (putatively, set by carbon abundance) is called $E(t)$, then cells each consuming energy at a rate of β energy units per cell per time collectively deplete $E(t)$ at rate $-\beta N(t)$; but this is balanced by a resupply $-\alpha \frac{dN}{dt}$ from currently dying cells, where α is the energetic yield per dead cell (and we recall that death makes $dN/dt < 0$). Thus, we have the dynamical description of the energy supply of the form

$$\text{carbon limitation:} \quad \frac{dE}{dt} = \underbrace{-\beta N(t)}_{\substack{\text{viable cells consume} \\ \text{maintenance energy}}} \underbrace{-\alpha \frac{dN}{dt}}_{\substack{\text{dying cells} \\ \text{donate energy}}} . \tag{3.1}$$

Assuming that the energy reaches a steady-state (quickly relative to the longer timescales over which cells meaningfully change abundance), namely $dE/dt = 0$, implies that

$$\text{per-capita death rate} \equiv \frac{1}{N(t)} \frac{dN}{dt} = -\frac{\beta}{\alpha}. \tag{3.2}$$

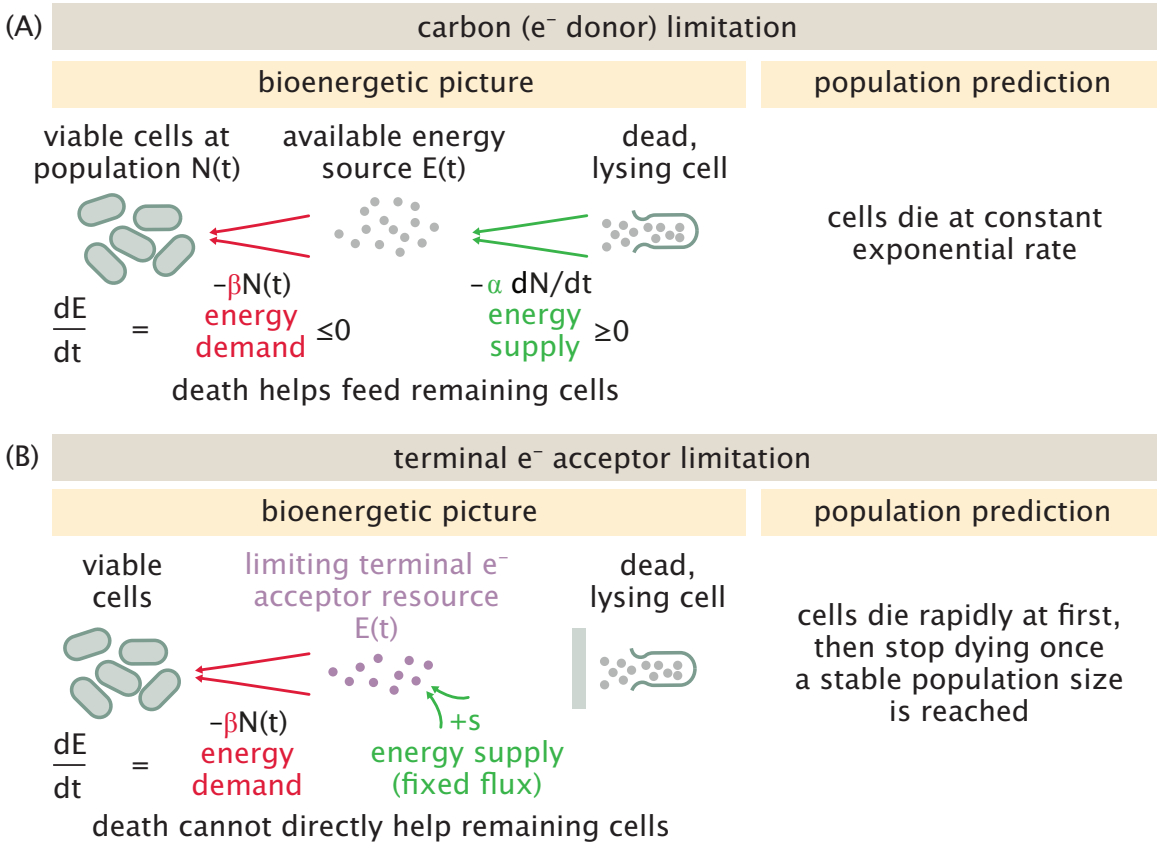

Figure 3.2: Distinct macroscopic physiology of death under deprivation of electron donor (e.g. carbon) versus deprivation of terminal electron acceptor (e.g. oxygen). (A) When cells are energy-limited by carbon, of which dying cells are made and can donate, viable cells can recycle nutrients from the "necromass" of their dying brethren and replenish their energy supply. The relevant energy source $E(t)$ changes in time due to consumption by cells at a rate $-\beta N(t)$ where β is the energy demand per time per cell, but replenished by dying cells at rate $\alpha\ dN/dt$ where α is the energetic content of a dead cell. (B) In contrast, when cells are limited by terminal electron acceptors (such as oxygen), dying cells do not meaningfully replenish the communal supply of the energetically-limiting resource. Instead a supply flux s fixed by environmental conditions participates in the energetic balance. Note that in these two cases, the putative nature of the limiting energetic resource has changed from the electron donor (grey dots in panel (A) to the electron acceptor (purple dots in panel (B)).)

This result gives the prediction that per-capita death rates should be constant in time, exactly the behavior affirmed by a straight line of abundance (measured on a log scale) versus time as shown in Figure 3.1(A). Since the slope of this death trajectory is proportional to the maintenance rate β at which bacteria consume energy, these curves can report precious information about the energetic status of cells. This conceit of inferring energetic status from death is useful and scalable, because a single viability experiment is relatively straightforward by the gymnastic standards of more complex microbiological measurements.

3.1.1 Generalizing energetic resource balance with cellular energy consumption under broader dynamics

When cells are limited by terminal electron acceptors such as in the absence of oxygen or molecules like oxidized phenazine, instead of carbon, we propose that dying cells do not substantially benefit the energetic state of their viable neighbors. This is because lysing cells are not generally significant sources of newly available terminal electron acceptors.[1] Instead, the supply of the limiting energetic resource is dictated by environmental boundary conditions distinct from dying cells, such as the flux of oxygen at a plane in a biofilm, or in the case of many recent experiments in the Newman laboratory [5], set by the action of the electrode reoxidizing extracellular phenazine. We illustrate this contrast in Figure 3.2(B).

This simple, foundational difference should drive very different macroscopic phenomenologies of death. Assume that the energetic pool $E(t)$ now interpreted differently as a pool largely set by terminal electron acceptor abundance, not carbon,

[1] At least, this statement appears appropriate for the externally-regulated extracellular redox carrier case of many of the experiments of interest in the Newman laboratory. Other physiological and environmental circumstances could change this picture and e.g. restore some dependence of the energetic supply term on dying cells.

changes in time as,

$$\text{terminal } e^- \text{ acceptor limitation: } \quad \frac{dE}{dt} = \underbrace{-\beta N(t)}_{\substack{\text{viable cells consume} \\ \text{maintenance energy}}} + \underbrace{s}_{\substack{\text{environment} \\ \text{supplies energy}}}, \tag{3.3}$$

where s is the rate at which energy is supplied by the environmental milieu.

Previously, in the carbon limitation case, dying cells replenished energetic resource at a rate $s = -\alpha \frac{dN}{dt}$. However, generically—and especially plausibly in the case of limited terminal electron acceptors—the supply rate will not just be proportional to the death rate. Instead, we observe that the supply rate s of the energetic resource resource can be some potentially physiologically or environmentally complex function of the instantaneous energetic resource $E(t)$; the instantaneous cell count $N(t)$; and/or the current rate of change of the cells dN/dt, namely,

$$\text{supply rate: } s \equiv s(N(t), E(t), dN/dt). \tag{3.4}$$

Immediate gifts from knowing energetic resource reaches steady-state

When the energy reaches a steady state $dE/dt = 0$[2], the coordinates $N(t), E(t)$, and dN/dt become subject to an implicit relation. That is, when the right side of Eq. 3.3 vanishes, the governing quantities s, N, E are constrained to depend on each other and jointly fall on some manifold specified by the shape of the supply rate function s, namely,

$$N(t) := \frac{s(N(t), E(t), dN/dt)}{\beta}. \tag{3.5}$$

[2]A steady-state in energy, $dE/dt \approx 0$, is often plausible over the timescales of the slower changes in the cell count $N(t)$. Specifically, for typical laboratory conditions of interest like those studied by Ciemniecki and coworkers [5] and Schink and coworkers [4], measurements typically report per-capita death rates on the order $\lesssim 1/\text{few per day}$; this timescale should be slow relative to the local equilibration of the molecular energy pool by uptake and metabolic reactions.

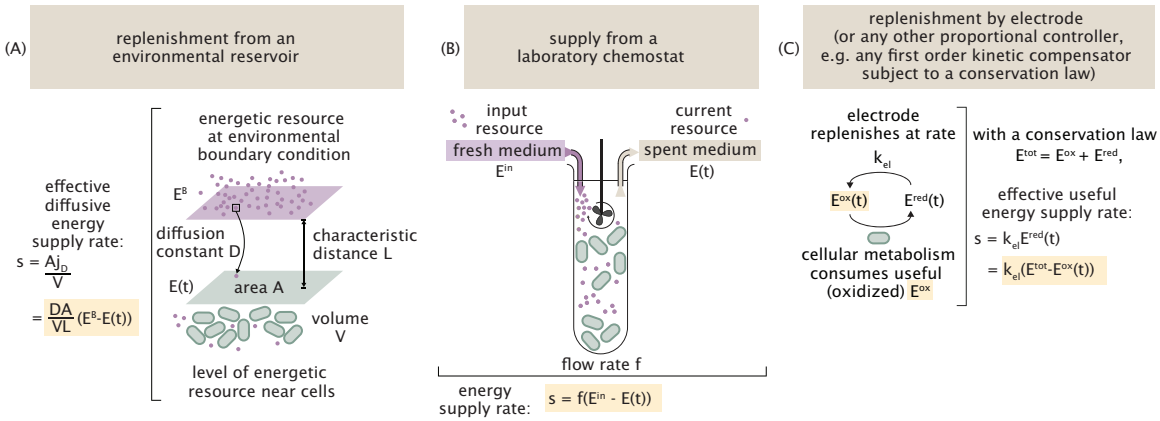

Figure 3.3: Diverse environmental and laboratory scenarios where energetic resources $E(t)$ are replenished at a supply rate s adopting the same linear mathematical form, $s(E(t)) = k(F - E(t))$, for some appropriate constants k, F. (A) If cells whose local abundance of energy is $E(t)$ are in contact with an environmental reservoir presenting a boundary condition of fresh energy resource at a higher concentration E^{B}, the typical diffusive current of resource to the body of cells can be modeled as $s = \frac{DA}{VL}(E^{\mathrm{B}} - E(t))$, where A and V are the characteristic area and volume of the cells; D is the diffusion coefficient of the energetic resource; and L is a characteristic distance between the cells and the environmental boundary condition. (B) A laboratory chemostat actively replenishing the abundance of energetic resources at current concentration $E(t)$ by flowing fresh medium at concentration E^{in} at flow rate f resupplies energy at a rate $s = f(E^{\mathrm{in}} - E(t))$. (C) When functional energetic resource is regenerated by a reaction mechanism with first-order kinetics in a depleted form of the resource, the supply rate of the functional form of the resource is proportional to the difference between the current abundance of functional resource and the total amount of resource. This example manifests in the setting of cells that need an energetic resource in its oxidized to accomplish metabolism; if an electrode reoxidizes reduced resource at rate k_{el}, then the supply term adopts the form $s = k_{\mathrm{el}}(E^{\mathrm{tot}} - E^{\mathrm{ox}}(t))$. (This scenario is discussed in much further mathematical and experimental detail shortly in §3.2.)

For suitably well-behaved supply rate functions s, this constraint can enable the determination of one of these quantities $\{E, N, dN/dt\}$ in terms of the other two—for instance, $N(t) = h(E, dN/dt)$ for some function h, and so on. This mathematical reasoning was exactly that which related N and dN/dt in the earlier simpler case of carbon limitation: there, the constraint simplified to $N = h(dN/dt)$ specified by the very simple proportionality between cell abundance and its time derivative, as highlighted in Eq. 3.2.

To illustrate how this constraint continues to deeply and quantitatively illuminate the population dynamics and energetic status of cells beyond the simple case of carbon limitation, we now specialize to the case where the energy supply term s depends linearly

on the present value of the energy $E(t)$, namely,

$$s \equiv s(E(t)) \equiv k(F - E(t)), \tag{3.6}$$

for some constants k and F. Here, k sets the timescale on which energy is resupplied, and F specifies the default, steady magnitude of the energy in the environment if no consumption by cells were occurring. As illustrated in Figure 3.3, this mathematical character emerges highly naturally and commonly across a variety of endogenous and laboratory environments for microbial cells. For instance, as depicted in Figure 3.3(A), if a cell population is in contact with an environmental reservoir delivering a boundary condition of fresh energetic resource (such as oxygen) at a larger concentration E^{B} than locally near the cells, the resulting concentration gradient can generate a diffusive current proportional to the difference between the concentration $E(t)$ near cells and the concentration found at the boundary. Specifically, Fick's law gives the diffusive flux as $j_D = -D\frac{\partial E}{\partial z}$ for an energetic resource with diffusion constant D varying in a spatial coordinate z; taking the concentration gradient as $\frac{\partial E}{\partial z} = \frac{E_B - E(t)}{L}$ if the cells are a characteristic distance L away from the environmental boundary gives the average rate at which the concentration of energy is replenished near the cells as $s = \frac{DA}{VL}(E^{\mathrm{B}} - E(t))$, where A and V are the area and volume of the cell population.

We contend that this transport scenario, which generically emerges from coupling to big external reservoirs, applies widely to important terminal electron acceptors across natural environments. Specifically, the atmosphere presents a huge, well-mixed store of oxygen that can generically encourage an oxygen-rich boundary condition over layers of soil on land, and water columns and sediments in oceans and freshwater. Accordingly, in surface

layers, soluble oxygen at levels set by Henry's law in equilibrium with the atmosphere[3] can provide a steady flux of oxygen to cells depleting it. Oxygen is hardly the only critical bioenergetic resource participating in nearly adiabatic exchange with large external reservoirs. Carbon dioxide (despite its low redox potential) is widely harnessed for metabolism and reduced by methanogenic archaea [10] and acetogenic bacteria [11, 12]. Dissolved sulfate at large ambient concentrations of few tens of millimolar [13] is also widely present across oceans and used by sulfate reducing bacteria. These examples—which span the dominant terminal electron acceptors enabling respiration across the globe—illustrate how atmospheric or hydraulic coupling to large external pools can drive replenishment of energetically-critical resources. In contrast, the most thermodynamically useful electron donor forms of carbon are less frequently backed by such well-mixed reservoirs, and can often instead arrive as finite boluses, solids and adsorbed species. Of course, this tendency for electron acceptors to be resupplied by large reservoirs and electron donors to arrive more finitely or episodically is hardly absolute. For instance, the nitrate crusts of deserts [14] and solid-phase iron minerals, built up over geological time as solids, can be as relatively non-renewable as fresh organic carbon. And, conversely, steady release of carbon from abiotic reservoirs or ecological crossfeeding can contribute steady streams of electron donors instead of finite pools. We highlight these archetypes simply to affirm that kinetic circumstances where metabolically-limiting resources arrive as steady supply fluxes (however slow) are extremely common across natural environments, and the physicochemical nature and abundance of electron acceptors make them particularly apt to exhibit these supply kinetics.

[3] Typical values of soluble oxygen are set by Henry's law; oxygen's Henry's law volatility constant is $H^{pc}_{V,O_2} \equiv \frac{p_{O_2}}{c_{O_2,aq}} \approx 770 \underbrace{\frac{L\,atm}{mol}}_{atm/molar}$ [8]. Since atmospheric oxygen is ≈20% of the atmosphere's composition, at 1 atmosphere oxygen's partial pressure is about $p_{O_2} \approx 0.2\ atm$. Thus we expect $c_{O_2,aq} \approx \frac{p_{O_2}}{H^{pc}_{V,O_2}} \approx \frac{0.2\ atm}{770/atm/molar} \approx 2.6\times10^{-4}\ M = 260\ \mu M$. This well agrees with values of oxygen measured at $c_\infty = 210\ \mu M$ at e.g. the surface of human mucus [9].

Joining these natural environments, common laboratory settings also deliver energy to cells at rates linear in the current energy supply. As shown in Figure 3.3(B), continuous flow chemostats flowing in fresh medium with resource at concentration E^{in} at volumetric flow rate f replenish energy at a net rate of $s = f(E^{\text{in}} - E(t))$. Alternatively, as shown in Figure 3.3(C), if the functional level E^{ox} of energetic resource is replenished by redox reactions accomplished by the environment or a reoxidizing laboratory electrode, first order kinetics in the reduced form of the resource and a conservation law implies that useful energy is resupplied at a rate $s = k_{\text{el}}E^{\text{red}}(t) = k_{\text{el}}(E^{\text{tot}} - E^{\text{ox}}(t))$, where k_{el} is the first-order oxidizing rate of the electrode and E^{tot} is the total extracellular concentration of the resource. We will return in much greater detail to experiments exploiting this latter technology to probe energy-limited physiology of *P. aeruginosa* in §3.2. More generally, we remark that the form of a linear dependence of s on the present resource level is precisely the form of a proportional integral control scheme; can develop from any coupled first order kinetics that share E as a substrate but generate it in the opposite direction as the cells consume it; or else can also emerge as any dynamical linear approximation to a departure from equilibrium in $E(t)$.

Now that a supply term is specified, we find the consequences of a steady-state in the overall functional energy dE/dt.[4] The rate of change of energy in Eq. 3.3 becomes

$$\frac{dE}{dt} = -\beta N(t) + k(F - E(t)) := 0 \tag{3.8}$$

$$\rightarrow E_{\text{ss}} = \boxed{F - \frac{\beta N(t)}{k}}. \tag{3.9}$$

Armed with this expression for the energy pool E_{ss}, we now ask for the consequences for

[4] Alternatively, if cells deplete energy $E(t)$ at a rate $\beta N(t)E(t)$—that is, first order in $E(t)$ instead of zeroth order—the steady state value of the energy is instead,

$$E_{\text{ss}}^{(1)} = F\frac{k}{k + \beta N(t)}. \tag{3.7}$$

how populations of cells change in time, dN/dt.

However, even by adopting a specific form for the supply term $s(E(t))$ and enforcing a steady-state in E does not deliver closed expression for dN/dt automatically. That is, in general we no longer automatically enjoy a closure of the system of equations that specifies how cell counts change in time given just how the energy supply changes in time. To make progress, we need to provide an extra theoretical ingredient: an *ansatz* for the form of dN/dt's dependence on E and N.

Closing the system of equations to predict dN/dt and $N(t)$, how viability changes over time

We will now hazard the audacity of such an *ansatz* (namely, a brazen quantitative guess). Often, the biochemical, environmental, and genetic context of cells under study will provide principled suggestions or clues for plausible functional forms for the population changes in time, dN/dt. However, absent more precise physiological information, one phenomenological way to proceed is to anticipate that dN/dt is a smooth function f of just the variables $N(t)$ and $E(t)$ (and time derivatives thereof), namely,

$$\frac{dN}{dt} = f\left(N(t), E(t), \frac{dE}{dt}, \dots\right). \tag{3.10}$$

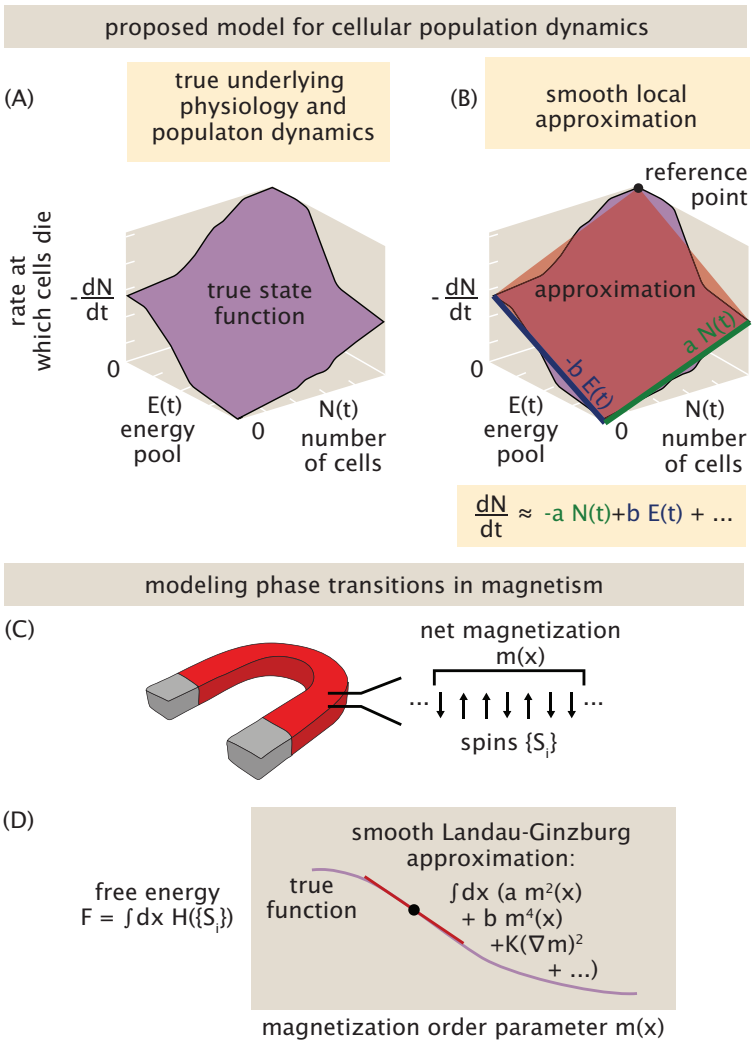

Figure 3.4: Model proposed to relate the rate of change dN/dt of the abundance of cells to the state variables of the current energy $E(t)$ and the current abundance of cells $N(t)$. (A) In principle, the rate that cells die can depend in complex ways on microscopic biochemical conditions of cells. We assume these dependencies can be subsumed into smoothly-varying dependencies on macroscopic state variables—an overall energy pool $E(t)$ (including possibly its time derivatives), and the current abundance of cells $N(t)$ (depicted schematically as the surface in purple). (B) When dN/dt varies smoothly in $N(t)$ and $E(t)$, it can admit a smooth local approximation as an expansion in each coordinate. The simplest expansion has the form $dN/dt = -a\ N(t) + b\ E(t)$, for constants $a, b \geq 0$ on physiological grounds (namely, more cells should cause death rate to increase; more energy should cause death rate to decrease). (C) This approach—approximating a macroscopic function of many microscopic variables (death rate) by low order expansions in mesoscopic state variables (current cell count and communal energy level)—is ratified by analogy to the success of the Landau-Ginzburg approach to phase transitions in (for instance) magnetic materials. In the Landau-Ginzburg approach, microscopic variables (magnetic spins $\{S_i\}$) are summarized by order parameters (including the magnetization $m(\mathbf{x})$), and the local Hamiltonian of the whole system is expressed as a Taylor expansion of the free energy density with respect to the order parameters and its derivatives, but only retaining terms permitted by physical symmetries in the problem. Keeping only the lowest non-trivial terms gives simple field equations consistent with the field variables and known constraints.

As illustrated in Figure 3.4, this formulation immediately invites a Taylor expansion, about some reference state $N(t) = N_*, E(t) = E_*$. In general, this gives,

$$f \approx f_0 + \left.\frac{\partial f}{\partial N}\right|_{N^*,E^*} (N - N_*) + \left.\frac{\partial f}{\partial E}\right|_{N^*,E^*} (E - E_*) + \frac{1}{2} \left.\frac{\partial^2 f}{\partial E \partial N}\right|_{N_*,E_*} (E - E_*)(N - N_*) + \cdots \tag{3.11}$$

$$= \underbrace{\left(f_0 - \frac{\partial f}{\partial N} N_* - \frac{\partial f}{\partial E} E_* + \cdots\right)}_{\equiv c} + \underbrace{\frac{\partial f}{\partial N}}_{\equiv -a} N + \underbrace{\frac{\partial f}{\partial E}}_{\equiv b} E + \frac{1}{2} \frac{\partial^2 f}{\partial E \partial N} N E + \cdots, \tag{3.12}$$

where we have defined constants a, b, and c as indicated for notational convenience, foreshadowing their expected physical signs.

If this function does not vary aggressively with its variables $N(t)$, $E(t)$, then it is reasonably approximated by truncating this series to the first few terms. Retaining various orders of terms in this expression amounts to different complexities acknowledged of physiology. This tradition is simple but validated by the expressiveness of both the generalized Lotka Volterra equations and consumer resource models of ecology[5] and a broader tradition of parsimonious expansions of macroscopic field variables throughout statistical physics (as illustrated by the analogy in Figure 3.4(C-D)).

For purposes of our immediate discussion here, however, we will consider the simplest linear theory of physiology, given by the first order terms in this expansion, namely

$$\frac{dN}{dt} \approx c - aN(t) + bE(t). \tag{3.13}$$

Now, we argue that on physiological grounds, we anticipate that $c = 0$ and $a, b \geq 0$—that

[5]For instance, taking $b = 0$ and $\frac{1}{2} \left.\frac{\partial^2 f}{\partial E \partial N}\right|_{N_*,E_*}$ nonzero gives a linear variant of the famous MacArthur Consumer Resource Model for one consumer and one resource (see Eq. A2 in Cui, Marsland, and Mehta [15]).

is, we expect that no change in the cell population should occur without any cells or energy ($N(t) = E(t) = 0$), and further that more cells should cause at most more death but more energy should cause at most less death. This gives,

$$\boxed{\frac{dN}{dt} \approx -aN(t) + bE(t)}. \tag{3.14}$$

The parameters a and b capture overall couplings of cellular death rate to current population size and energy states as shown by the approximate red plane in Figure 3.4(B) and carry natural physical meanings. The constant a represents the per-capita death rate (e.g. exponential death rate) if no excess available resource E were available, $E = 0$; it is reasonable to expect that a monotonically increases with the basal metabolic rate of cells β. Conversely, the energy coefficient b represents the decrease in the number of cells dying per time (eg the unit change in dN/dt) expected per additional unit of energy; it should be related to the thermodynamic yield/biochemical quality of the energetic resource in question. Just as for the coefficients entering Landau-Ginzburg field theory of critical phenomena, these parameters are phenomenological but, in principle, directly experimentally measurable, and their qualitative features can be integrated with thermodynamic understanding. For instance, different electron donors and acceptors fall on a hierarchy based on the reducing or oxidizing potential of their half reactions, in addition to the biochemical efficiency with which given organisms accomplish these reactions for given resources. Accordingly, different energetic resources should impose a corresponding hierarchy on the numerical values of the parameters b.

Finally, armed with both the consequences of an energetic steady-state in Eq. 3.9 and the proposed closure of the systems of equations governing cell count and energy Eq. 3.14, we solve how cell count changes over time. Substituting the expression for energy into the

proposed dN/dt gives,

$$\frac{dN}{dt} = -aN(t) + b\underbrace{E(t)}_{\equiv E_{ss}} \tag{3.15}$$

$$= -aN(t) + b\left(F - \frac{\beta N(t)}{k_{\text{el}}}\right) \tag{3.16}$$

$$= -\left(a + \frac{\beta}{k_{\text{el}}}\right)N(t) + bF. \tag{3.17}$$

This differential equation for the abundance of cells Eq. 3.17 has a simple, easily expressed analytical solution, predicting that cell count will change in time according to,

$$N(t) = \boxed{\underbrace{\frac{bF}{a + \frac{\beta}{k}}}_{\equiv N_\infty} + \left(N_0 - \frac{bF}{a + \frac{\beta}{k}}\right)\exp\left[-\left(a + \frac{\beta}{k}\right)t\right]} \tag{3.18}$$

$$= N_\infty + (N_0 - N_\infty)\exp\left[-\left(a + \frac{\beta}{k}\right)t\right], \tag{3.19}$$

where N_0 is the initial population of cells at time $t = 0$. These population dynamics in Eq. 3.19 reflect an exponential decay to a constant, nonzero, steady-state population size,

$$N_\infty \equiv \frac{bF}{a + \frac{\beta}{k}}. \tag{3.20}$$

This steady-state population scales linearly with the parameter b setting the reduction in death rate per unit of excess energy and the default environmental value F of the energy (if no cells were consuming energy). It also increases (hyperbolically) with the rate k at which energy is resupplied. In contrast, this steady-state population decreases with the default per-capita death rate a (if no energy were present) and the maintenance rate β at which cells consume energy. Notice that the dynamics of this solution Eq. 3.19 interpolates between two slopes for log survival: at early times, if $N(t)$ is far above the steady-state abundance,

the population declines approximately exponentially with a slope $a + \frac{\beta}{k}$ in time. At late times, however, the approach to a the constant steady-state population flattens this slope, asymptotically converging to zero.

To illustrate that this model, however extraordinarily simple, nonetheless makes precise and falsifiable predictions that commune with real measurements, we return to the motivating abundance curves of Fig. 3.2(B), measured by Ciemniecki and coworkers [5]. In this (carbon-plush, anaerobic) setting, oxidized phenazine is the limiting energetic resource, which invites us to mathematically identify it as setting the variable $E(t)$ in our preceding equations, $E(t) \sim [\mathrm{PCN}]^{\mathrm{ox}}(t)$. Under the conditions of the indicated measurements, explained much more thoroughly in the following section, we anticipate that the action of an electrode accomplishing the measurement replenishes the oxidized phenazine at a first order rate in the current amount of reduced phenazine. This identifies the default amount F of resource (phenazine) if the cells were absent as the total amount of phenazine, $F = [\mathrm{PCN}]^{\mathrm{tot}} = [\mathrm{PCN}]^{\mathrm{ox}}(t) + [\mathrm{PCN}]^{\mathrm{red}}(t)$. Armed with these interpretations, our model of Eq. 3.20 makes the strong and unambiguous prediction that the late-time (approximating steady-state) population size of cells should scale linearly with the total phenazine concentration,

$$\text{prediction: } N_{ss} \propto [\mathrm{PCN}]^{\mathrm{tot}}. \tag{3.21}$$

Is this prediction ratified? Fig. 3.5 largely affirms this prediction, registering an impressively linear variation of total population size at late times with external phenazine concentration.

Moreover, importantly, the model also adequately describes the fuller dynamics of

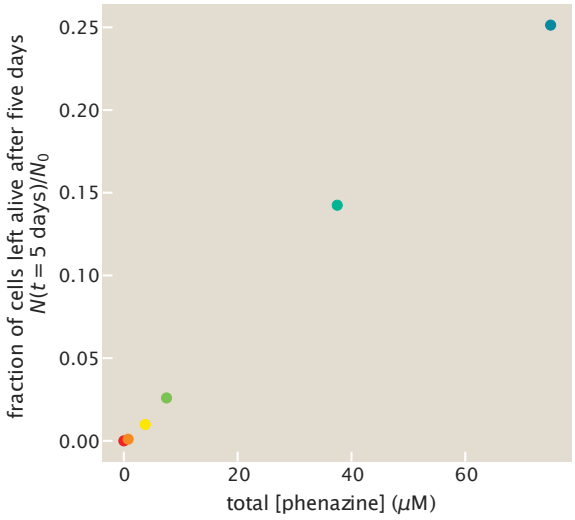

Figure 3.5: Remaining abundance of cells at late times (at $t = 5$ days), as a function of the extracellular phenazine concentration, extracted from the data depicted earlier in Fig. 3.2(B) from Ciemniecki *et al.* [5]. Late cell abundance clearly varies largely linearly with external phenazine concentration. Note the small departure from linearity visible in the condition at 75 μ phenazine at the upper right, which might be interpretable as the onset of physiological saturation or toxicity. Another mild departure is visible for the condition without phenazine entirely (red dot at lower left), since our model does not comment on the nature of energy sources orthogonal to phenazine.

survival curves, as supported by Fig. 3.6.[6]

The adequate agreement of even the simplest model we discussed and both quantitative and qualitative features of these population abundance curves over time invites both optimism for broader applicability and extensions. These models connect, in a minimally viable way, the unique phenomenology and underlying bioenergetic status of cells

[6]To resolve the two remaining fit parameters for this model's prediction for $N(t)$, we can rewrite the prediction assuming that the only parameter varying was F (set by the total phenazine concentration) and not the physiological or electrode parameters a, b, k, β. Dividing Eq. 3.18 by N_0 gives,

$$\text{fractional viability}: \frac{N(t)}{N_0} = \frac{bF}{N_0\left(a+\frac{\beta}{k}\right)} + \left(1 - \frac{bF}{N_0\left(a+\frac{\beta}{k}\right)}\right)\exp\left[-\left(a+\frac{\beta}{k}\right)t\right]. \tag{3.22}$$

Assuming fixed b, N_0, a, β, k but varying F, we can define

$$\frac{N(t)}{N_0} = \sigma F + (1-\sigma F)\exp\left[-\frac{\xi}{\sigma}t\right], \tag{3.23}$$

where we appealed to just two parameters $\sigma \equiv \frac{b}{N_0(a+\beta/k)}$ and $\xi \equiv b/N_0$. Note that to model death requires that $(1 > \sigma F)$.

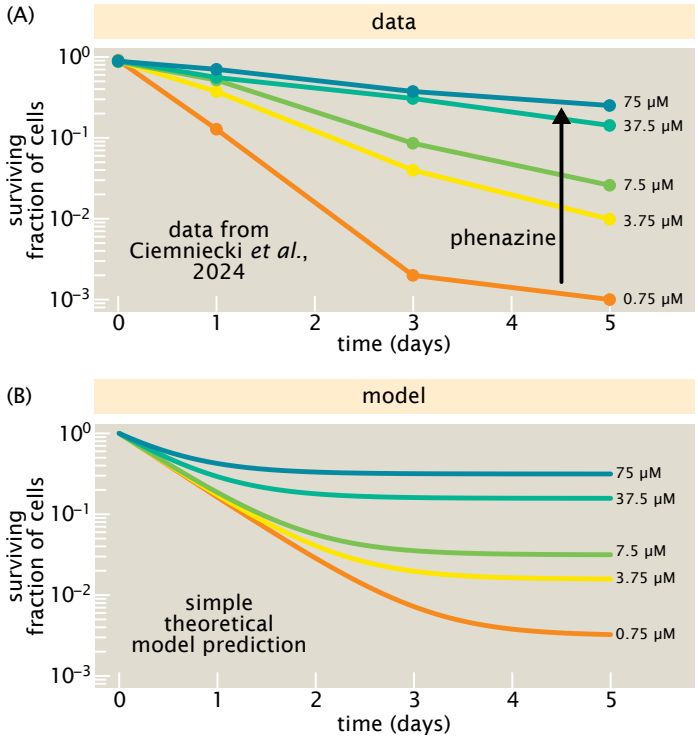

Figure 3.6: Measured survival data compared to the model of Eq. 3.19. (A) A physiologically tolerated subset of data. (B) Our simplest model prediction from Eq. 3.17, enforcing the energy source term F proportional to the phenazine concentration (otherwise leaving two fit parameters).

challenged by limited terminal electron acceptors. Once paired with appropriate calibrating experiments and measurements, such models could infer and monitor the metabolic rates of cells scalably across environmental conditions and perturbations, similarly to how such inferences have been developed and productively applied to the case of carbon limitation.

3.2 Explicit kinetic theories for maintenance experiments

Having seen that both qualitative and quantitative features of how cells survive when limited by terminal electrode acceptors can be predicted from a very simple model with interpretable physiological parameters, we now strive to make close contact with particular culturing experiments. Specifically, we aim to build candidate "theories of the experiment" for how the raw measured quantities (metabolic current and cell abundance) interact in experiments on *Pseudomonas* sustained anaerobically [5] in the Newman laboratory. Our aim is practical and granular: we want to offer distinct predictions for observables that help distinguish between different possible underlying kinetic pictures that could describe how cells and experimental electrodes interact. We feel that adjudicating among these underlying kinetic pictures is important to interpret exactly how trends in observables report on underlying physiology. However, while we now specialize to the language of *Pseudomonas*, phenazines, and electrodes in what follows, we underscore that essentially identical mathematics would make quantitative predictions of a plethora of broader environmental scenarios, such as those intimated in Fig. 3.3, *mutatis mutandis*.

At a high conceptual level, eliding many fascinating and complex biochemical details, cells produce energy by directing electrons from an electron donor (e.g. a carbon source like a sugar) and enzymatically delivering these electrons to an electron acceptor (such as oxygen in aerobic conditions), gleaning Gibbs free energy of the coupled half reactions

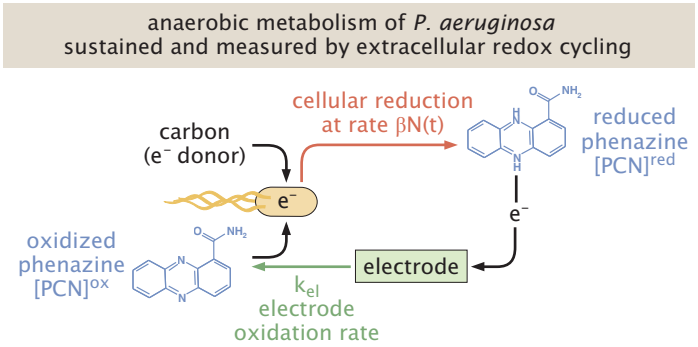

Figure 3.7: Schematic for how cellular metabolism at rate $\beta N(t)$, driving reduction of extracellular phenazine, is counteracted by oxidation by the electrode at rate k_{el}.

along the way. Oxygen is often a privileged electron acceptor for many aerobe species. Yet, when it is unavailable—as is exceedingly common in microbial biofilms in soil, mucus-filled lungs, marine sediments, and beyond—cells have developed a spectrum of ingenious alternative energy conservation strategies. One such tactic is implemented by *Pseudomonas*, whose strains can produce a class of extracellular redox-active molecules known as phenazines. Often, producing phenazines is key to how *Pseudomonas* can persist and exhibit pathogenicity, despite energy limitation or antibiotics, across natural environments.

To explore the beautiful metabolic dynamics attending anaerobic situations compensated for by phenazines, cells where the natural phenazine biosynthesis pathways have been knocked out ($\Delta phz1/2$ strains) can be provided titrated amounts of exogenous extracellular phenazine. As discussed in both recent [5] and now-classic [16, 17] studies, while these struggling cells perform basal metabolism and reduce extracellular phenazine as a terminal electron acceptor, an electrode can reoxidize phenazine to replenish its supply and simultaneously offer a readout of cellular metabolism. We illustrate this procedure in Fig. 3.7. Further, under some relevant physiological conditions, calibrations and biochemistry establish that 1 electron per second per cell measured by electrode can correspond to the energetic equivalent of a cell spending $\sim$1 ATP hydrolysis's worth of

energy [5]. Thus, measured current gives an unprecedentedly direct readout of cellular metabolism in a variety of challenging conditions of enduring environmental relevance—namely, anaerobic energy limitation.

Now, we strive to minimally mathematize such cellular metabolism balanced by electrode kinetics. Specifically, we model cells as reducing oxidized phenazine in either a zeroth order process (that is, cells reduce oxidized phenazine at a rate independent of the current level of oxidized phenazine), or as a first order process (that is, the rate at which oxidized phenazine is reduced scales with the current concentration of oxidized phenazine). Complementarily, we model the electrode as accomplishing reduction that is either zeroth order or first order in the current level of reduced phenazine in the culture medium.

These different kinetic orders are each plausibly well justified in different physiological and physical scenarios. Cells would reduce oxidized phenazine at a constant rate (zeroth order in the external phenazine) if their internal metabolic repertoire, not uptake per se, bottlenecks cellular reduction, and/or if their emission of reduced phenazine itself is saturated. Alternatively, however, if uptake or transport were limiting cellular metabolism, reduction kinetics would more plausibly be dependent on (plausibly first order in) the level of oxidized phenazine. Analogously, if transport to the electrode were truly limiting the rate at which it could reoxidize phenazine, the electrode would plausibly depend on the current level of reduced phenazine (credibly to first order, for example in a diffusion-limited sense). Otherwise, if the electrode's internal kinetics were a bottleneck, its action would better be described as zeroth order.

It is not fundamentally obvious, *a priori*, that the operating regimes of microbial culture (or environmental settings) necessarily ordain that any of these kinetic scenarios is never relevant. (This said, to interpret the electrode as measuring something about the ambient metabolic environment, its current is probably not zeroth order (which would register a constant current no matter the action of cells).) That is, there may be physical scenarios

where any of these kinetic combinations manifest. In particular, a combination of these scenarios might develop simultaneously in natural biofilms or planktonic cultures.

Accordingly, here, we specify, solve, and explore all four sets of kinetic equations setting the balance between cellular reduction of phenazine and the reoxidation by an electrode up to first order reaction kinetics in each process. These joint models are anticipated in Figure 3.8.

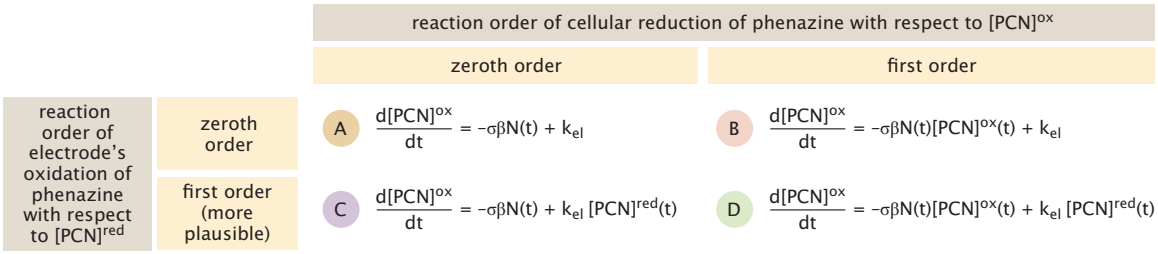

Figure 3.8: Presiding differential equations for the functional energy source. All four kinetic order combinations possible when cells and electrodes each engage in zeroth or first order kinetics in their respective substrate forms of phenazine. (A) Zeroth order kinetics by cells, zeroth order kinetics by the electrode. (B) First order kinetics by cells, zeroth order kinetics by the electrode. (C) Zeroth order kinetics by cells, first order kinetics by the electrode. (D) First order kinetics by cells, first order kinetics by the electrode. (Note that across these models, the units of the presiding constants change according to dimensional consistency: e.g. σ carries units of phenazine reduced per second per joule metabolized by cells if cells are zeroth order, but alternatively has units of per second per joule metabolized by cell if cells are first order in oxidized phenazine. Analogously, k_{el} has units of oxidized phenazine produced per time if the electrode is zeroth order, but otherwise has units of oxidized phenazine molecules per reduced phenazine per time if the electrode is first order.)

We discuss models (C) and (D) previewed in Fig. 3.8, corresponding to first order kinetics by the electrode, first and in greatest detail. These are the especially relevant and interesting cases where the electrode's activity actually varies with the present concentration of oxidized phenazine. However, for completeness, we include and remark in passing on aspects of the solutions of models (A) and (B) (which reflect zeroth order kinetics by the electrode).

model (C)	
cells: zeroth order in $[PCN]^{ox}$ electrode: first order in $[PCN]^{red}$	
differential equation:	$\frac{d[PCN]^{ox}}{dt} = -\sigma\beta N(t) + k_{el}[PCN]^{red}(t) = -\sigma\beta N(t) + k_{el}([PCN]^{tot} - [PCN]^{ox}(t)) = -\sigma\beta N(t) - k_{el}[PCN]^{ox}(t) + k_{el}([PCN]^{tot}$ (of the form dx/dt = − a N(t) − b x(t) + c)
resulting solution:	$[PCN]^{ox}(t) = \exp[-k_{el}(t)]\left([PCN]_0^{ox} + \int_0^t d\tau \exp[k_{el}\tau](k_{el}[PCN]^{tot} - \sigma\beta N(\tau))\right)$
simplification if N(t) is ≈ constant N_0:	$[PCN]^{ox}(t) = \exp[-k_{el}(t)]\left([PCN]_0^{ox} - \left([PCN]^{tot} - \frac{N_0\sigma\beta}{k_{el}}\right)\right) + \left([PCN]^{tot} - \frac{N_0\sigma\beta}{k_{el}}\right)$
steady-state PCN:	$[PCN]_\infty^{ox} = [PCN]^{tot} - \frac{\sigma\beta N(t)}{k_{el}}$
steady-state current:	$I_{ss} \propto k_{el}\left([PCN]^{tot} - \left([PCN]^{tot} - \frac{\sigma\beta N(\tau)}{k_{el}}\right)\right) = \sigma\beta N(t)$
per-cell steady-state current:	$\frac{I_{ss}}{N(t)} \propto \sigma\beta$

Figure 3.9: Mathematical properties of Model (C) (as portended by Fig. 3.8).

3.2.1 Model C: Zeroth-order cells fed by first-order electrodes

Back in Eq. 3.8, we visited a form of this model, evaluated when the energetic resource (e.g. oxidized phenazine) reached a steady-state. Here we return to set up the scenario and probe some of its more dynamical properties in the explicit setting of cells sustained by extracellular phenazine cycling.

As Fig. 3.7 recalls, phenazine transitions between two chemical forms, oxidized ($[PCN]^{ox}$) or reduced ($[PCN]^{red}$), with total phenazine concentration giving the total $[PCN]^{tot} = [PCN]^{ox} + [PCN]^{red}$. Assume cells reduce phenazine at a constant rate $\sigma\beta N(t)$; namely, proportional to their total maintenance energy demand $\beta N(t)$, where β is the basal metabolic power per cell (in e.g. ATP/s/cell or Watt/cell), $N(t)$ is their current abundance, and σ describes the number of phenazine reductions required per unit of energy. If electrodes replenish the oxidized form of phenazine at a first-order rate in the current level of reduced phenazine, $k_{el}[PCN]^{red}(t)$, then the competition of these reactions sets how the current level of oxidized phenazine changes in time, namely,

$$\frac{d[\mathrm{PCN}]^{\mathrm{ox}}}{dt} = \underbrace{-\sigma\beta N(t)}_{\text{cells reduce oxidized phenazine}} + \underbrace{k_{\mathrm{el}}[\mathrm{PCN}]^{\mathrm{red}}}_{\text{electrode reoxidizes phenazine}} = -\frac{d[\mathrm{PCN}]^{\mathrm{red}}}{dt} \tag{3.24}$$

$$= -\sigma\beta N(t) + k_{\mathrm{el}}([\mathrm{PCN}]^{\mathrm{tot}} - [\mathrm{PCN}]^{\mathrm{ox}}(t)). \tag{3.25}$$

At steady-state in the phenazine level, $\frac{d[\mathrm{PCN}]^{\mathrm{ox}}}{dt} = 0$, this differential equation predicts a stable level of oxidized phenazine given by,

$$[\mathrm{PCN}]^{\mathrm{ox}}_{\infty} = [\mathrm{PCN}]^{\mathrm{tot}} - \frac{\sigma\beta N(t)}{k_{\mathrm{el}}}. \tag{3.26}$$

The electrode reports a current, $I(t)$, proportional to the rate at which it is taking electrons off of reduced phenazine. We specified that rate to be $k_{\mathrm{el}}[\mathrm{PCN}]^{\mathrm{red}}(t)$ (by proscribing first order kinetics to the electrode). So, at steady-state in the oxidized phenazine concentration, the current will be,

$$I_{\mathrm{ss}} \propto k_{\mathrm{el}} \left([\mathrm{PCN}]^{\mathrm{tot}} - \left([\mathrm{PCN}]^{\mathrm{tot}} - \frac{\sigma\beta N(t)}{k_{\mathrm{el}}} \right) \right) \tag{3.27}$$

$$= \sigma\beta N(t). \tag{3.28}$$

Accordingly, this model makes the firm prediction that the measured per-cell current, $I_{ss}/N(t) \propto \sigma\beta$, should be proportional only to the maintenance rate that cells consume energy (thereby reducing phenazine); this steady-state current should *not* vary with the absolute population size $N(t)$, the total phenazine concentration $[\mathrm{PCN}]^{\mathrm{tot}}$, or the characteristic rate at which the electrode performs oxidation, k_{el}. As we will now see, these invariances are not assured for other kinetic scenarios.

More dynamically, if we knew $N(t)$ as a trajectory in time (despite its fundamental dependence on $E(t)$ itself), we could write an (implicit) closed form solution to this

differential equation Eq. 3.25, via an integrating factor. The result is the not-very-illuminating expression,

$$[\text{PCN}]^{\text{ox}}(t) = \exp[-k_{\text{el}}t]\left([\text{PCN}]_0^{\text{ox}} + \int_0^t d\tau \exp[k_{\text{el}}\tau]\left(k_{\text{el}}[\text{PCN}]^{\text{tot}} - \sigma\beta N(\tau)\right)\right). \quad (3.29)$$

However, this equation becomes more comprehensible and informative when the cell count $N(t)$ is essentially constant, $N(t) \approx N_0$, over the timescale over which we are asking dynamical questions of $[\text{PCN}]^{\text{ox}}(t)$. Then, phenazine relaxes in time as,

$$[\text{PCN}]^{\text{ox}}(t) = \exp\left[-k_{\text{el}}t\right]\left([\text{PCN}]_0^{\text{ox}} - \left([\text{PCN}]^{\text{tot}} - \frac{N_0\sigma\beta}{k_{\text{el}}}\right)\right) + \left([\text{PCN}]^{\text{tot}} - \frac{N_0\sigma\beta}{k_{\text{el}}}\right). \quad (3.30)$$

These properties of this model, which must be ruthlessly compared with behaviors registered by experiments, are summarized in Fig. 3.9.

3.2.2 Model D: First-order cells fed by first-order electrodes

When microbes also perform redox chemistry with phenazines with first order kinetics, the cellular term that was $-\sigma\beta N(t)$ in Eq. 3.25 becomes $-\sigma\beta N(t)E(t)$[7]. This yields the differential equation,

$$\frac{d[\text{PCN}]^{\text{ox}}}{dt} = \underbrace{-\sigma\beta N(t)[\text{PCN}]^{\text{ox}}}_{\text{cells reduce oxidized phenazine}} + \underbrace{k_{\text{el}}[\text{PCN}]^{\text{red}}}_{\text{electrode reoxidizes phenazine}} = -\frac{d[\text{PCN}]^{\text{red}}}{dt} \quad (3.31)$$

$$= -\sigma\beta N(t)[\text{PCN}]^{\text{ox}} + k_{\text{el}}([\text{PCN}]^{\text{tot}} - [\text{PCN}]^{\text{ox}}) \quad (3.32)$$

$$= k_{\text{el}}[\text{PCN}]^{\text{tot}} - (\sigma\beta N(t) + k_{\text{el}})[\text{PCN}]^{\text{ox}}. \quad (3.33)$$

[7]Notice here that the units of σ have changed between these two models, as required by dimensional consistency.

At steady-state in the balance of reduced contra oxidized phenazine, we see that

$$[\mathrm{PCN}]^{\mathrm{ox}}_{\infty} = [\mathrm{PCN}]^{\mathrm{tot}} \frac{k_{\mathrm{el}}}{k_{\mathrm{el}} + \sigma\beta N(t)}. \tag{3.34}$$

This implies that the electrode will report a steady-state current,

$$\begin{aligned} I_{\mathrm{el}} &\propto k_{\mathrm{el}}[\mathrm{PCN}]^{\mathrm{red}} && (3.35)\\ &= k_{\mathrm{el}}([\mathrm{PCN}]^{\mathrm{tot}} - [\mathrm{PCN}]^{\mathrm{ox}}) && (3.36)\\ &= k_{\mathrm{el}} \left([\mathrm{PCN}]^{\mathrm{tot}} - [\mathrm{PCN}]^{\mathrm{tot}} \frac{k_{\mathrm{el}}}{k_{\mathrm{el}} + \sigma\beta N(t)} \right) && (3.37)\\ &= k_{\mathrm{el}}[\mathrm{PCN}]^{\mathrm{tot}} \left(\frac{\sigma\beta N(t)}{k_{\mathrm{el}} + \sigma\beta N(t)} \right), && (3.38) \end{aligned}$$

Here, doubling the cell count has a multiplicative effect smaller than a doubling of the current. Only when $k_{\mathrm{el}} \gg \sigma\beta N(t)$ is the measured current approximately proportional to the cell count $N(t)$, $I_{\mathrm{el}} \propto \approx k_{\mathrm{el}}[\mathrm{PCN}]^{\mathrm{tot}} \frac{\sigma\beta N(t)}{k_{\mathrm{el}}} = [\mathrm{PCN}]^{\mathrm{tot}} \sigma\beta N(t)$. That is, the value of the current normalized by the total cell count, $\frac{I_{\mathrm{el}}}{N(t)}$, only enjoys the interpretation of being literally proportional to the per-cell metabolic rate β we are interested in when the electrode's reoxidation rate k_{el} is much faster than the cellular rate $\sigma\beta N(t)$.[8]

[8] A casual empirical remark included in Ciemniecki *et al.* [5] might be consistent with this picture: "Accordingly, on day 5 of the survival assay, we pooled ΔPCN1/2 cells from multiple technical replicate wells in the 375 mM PCN condition, pelleted them, resuspended them in a small volume, and added them to other wells containing ΔPCN1/2 cells and 375 mM PCN such that the total cell concentration was approximately doubled. We observed a 1.5x increase in current generation following the increase in cells that was sustained for at least 10 h (Figure S4B), demonstrating that the electrode was not limiting. Accordingly, the observed PCN oxidation rate at the electrode (Figure 5D) can be interpreted as equivalent to the cellular PCN reduction rate."

model (D)		
cells:	first order	in $[PCN]^{ox}$
electrode:	first order	in $[PCN]^{red}$

differential equation:	$\frac{d[PCN]^{ox}}{dt} = -\sigma\beta N(t)[PCN]^{ox}(t) + k_{el}\,[PCN]^{red}(t)$ $= -\sigma\beta N(t)[PCN]^{ox} + k_{el}\,([PCN]^{tot} - [PCN]^{ox}(t))$ (of the form $dx/dt = a - f(t)\,x(t)$) $= k_{el}[PCN]^{tot} - (\sigma\beta N(t) + k_{el})[PCN]^{ox}(t)$
resulting solution:	$[PCN]^{ox}(t) = \exp\,[-k_{el}(t)]\,\exp\left[-\sigma\beta\int_0^t d\tau\, N(\tau)\right]\left([PCN]_0^{ox} + k_{el}[PCN]^{tot}\int_0^t d\tau\,\exp\,[k_{el}\tau]\,\exp\left[\int_0^t ds\, N(s)\right]\right)$
simplification if N(t) is ≈ constant N_0:	$[PCN]^{ox}(t) = [PCN]^{tot}\,\frac{k_{el}}{k_{el}+\sigma\beta N_0} + \left([PCN]_0^{ox} - [PCN]^{tot}\,\frac{k_{el}}{k_{el}+\sigma\beta N_0}\right)\exp\,[-\,k_{el} + \sigma\beta N_0)t]$
steady-state PCN:	$[PCN]_\infty^{ox} = [PCN]^{tot} - \frac{k_{el}}{k_{el}+\sigma\beta N(t)}$
steady-state current:	$I_{ss} \propto k_{el}\,[PCN]^{tot}\left(\frac{\sigma\beta N(t)}{k_{el}+\sigma\beta N(t)}\right)$
per-cell steady-state current:	$\frac{I_{ss}}{N(t)} \propto k_{el}\,[PCN]^{tot}\left(\frac{\sigma\beta}{k_{el}+\sigma\beta N(t)}\right)$

Figure 3.10: Mathematical properties of Model (D) (as portended by Fig. 3.8).

This has the solution, assuming that $N(t)$ does not rapidly change over timescale of interest, namely $N(t) \approx N_0$,

$$[\mathrm{PCN}]^{\mathrm{ox}}(t) = \underbrace{[\mathrm{PCN}]^{\mathrm{tot}} \frac{k_{\mathrm{el}}}{k_{\mathrm{el}} + \sigma\beta N_0}}_{[\mathrm{PCN}]^{\mathrm{ox}}_{\infty}} + \left([\mathrm{PCN}]^{\mathrm{ox}}_0 - [\mathrm{PCN}]^{\mathrm{tot}} \frac{k_{\mathrm{el}}}{k_{\mathrm{el}} + \sigma\beta N_0}\right) \exp[-(k_{\mathrm{el}} + \sigma\beta N_0)t] \tag{3.39}$$

$$= [\mathrm{PCN}]^{\mathrm{ox}}_{\infty} + ([\mathrm{PCN}]^{\mathrm{ox}}_0 - [\mathrm{PCN}]^{\mathrm{ox}}_{\infty}) \exp[-(k_{\mathrm{el}} + \sigma\beta N_0)t]. \tag{3.40}$$

Notice that if there is a rapid steady-state in the phenazine dynamics (e.g. phenazine rapidly adjusts to a steady-state upon slower changes to cell counts), then

$$[\mathrm{PCN}]^{\mathrm{ox}} \longrightarrow [\mathrm{PCN}]^{\mathrm{ox}}_{\infty} = [\mathrm{PCN}]^{\mathrm{tot}} \frac{k_{\mathrm{el}}}{k_{\mathrm{el}} + \sigma\beta N(t)};$$

this holds instantaneously, even if $N(t)$ is not literally a constant N_0. This expression for the steady-state concentration of oxidized phenazine is illuminating from the perspective of our bioenergetic questions, since it anticipates a linear scaling of the oxidized phenazine concentration with total external phenazine, and also a hyperbolic (saturating) dependence on the current cell abundance $N(t)$. Further mathematical behaviors are summarized in Fig. 3.10.

3.2.3 Models A and B: Zeroth-order electrodes feed cells

Mathematical features of Models A and B are summarized in Figs. 3.11 and 3.12.

model (A)		
cells:	zeroth order	in $[PCN]^{ox}$
electrode:	zeroth order	in $[PCN]^{red}$

differential equation:	$\frac{d[PCN]^{ox}}{dt} = -\sigma\beta N(t) + k_{el}$ (of the form dx/dt = − a N(t) + c)
resulting solution:	$[PCN](t) = k_{el}t - \sigma\beta \int_0^t dt\, N(t)$
steady-state implication:	$N(t) = \frac{k_{el}}{\sigma\beta}$ (constant population size)
implied current:	constant $I_{ss} \propto k_{el}$ (independent of cell number N(t) or PCN)

Figure 3.11: Model (A) (as portended by Fig. 3.8).

model (B)	
	cells: first order in $[PCN]^{ox}$ electrode: zeroth order in $[PCN]^{red}$
differential equation:	$\frac{d[PCN]^{ox}}{dt} = -\sigma\beta N(t)[PCN]^{ox}(t) + k_{el}$ (of the form dx/dt = − a x(t) N(t) + c)
resulting solution:	$[PCN]^{ox}(t) = \exp\left[-\sigma\beta\int_0^t dt\, N(t)\right]\left([PCN]_0^{ox} + k_{el}\int_0^t d\tau \exp\left[\sigma\beta\int_0^\tau ds\, N(s)\right]\right)$
simplification if N(t) is ≈ constant N_0:	$[PCN]^{ox}(t) = \frac{k_{el}}{\sigma\beta N_0} + \left([PCN]_0^{ox} - \frac{k_{el}}{\sigma\beta N_0}\right)\exp\left[-\sigma\beta N_0 t\right]$
steady-state PCN:	$[PCN]_\infty^{ox}(t) = \frac{k_{el}}{\sigma\beta N(t)}$
implied current:	constant $I_{ss} \propto k_{el}$ (independent of cell number N(t) or PCN)

Figure 3.12: Model (B) (as portended by Fig. 3.8).

In summary, we expect that Model C or Model D may be especially effective models that quantitatively capture the phenazine dynamics and culturing experiments performed by the Newman laboratory. Which model is more appropriate demands targeted measurements, probably involving the independent measurement of the electrode's kinetic rate k_{el} itself, and asking at high resolution how current varies systematically with modulated properties like total cell count and total phenazine content in a spectrum of conditions. It is also very feasible to generalize these dynamics to a smooth interpolation of these models. For instance, cells implementing Michalis Menten kinetics at a rate $N(t)\beta_{\max}\frac{E(t)}{E(t)+K_M}$ (for resource $E(t)$, characteristic saturation constant K_M setting the typical onset of reductive activity, and maximum per-capita reduction rate $\beta_{\max}$) interpolates between zeroth and first order kinetics in energetic resource (namely phenazine).

3.3 Quantitative glimpses of metabolic adaptation to ionic stress in *Pseudomonas*

In the preceding chapter, we discussed how to newly extract from published death data [4] a coefficient—referred to as κ—specifying how much additional metabolic power *E. coli* cells spend per unit of environmental salt (sodium chloride). Under these aerobic, carbon-limited conditions, we inferred $\kappa_{E.\,coli} \sim 10^3$ ATP/s/cell/(mM NaCl). This large value betrays that *E. coli* can feel a considerable metabolic burden when buffeted by environmentally-feasible fluctuations in ion concentrations. Do other species, such as energy-limited *Pseudomonas*, show a comparably big sensitivity to its osmotic environment? How does their metabolic responses to environmental salt conditions change with other variables of environmental context?

Towards these questions, we worked with members of the Newman laboratory

(specifically Hannah Jeckel, Tracy (Chia Lun) Ho, Kemal Demirer) to design experiments, which they intrepidly performed, to measure the impacts of both extracellular salt and phenazine concentrations on the viability and metabolic rates of *P. aeruginosa* narrowly surviving in anaerobic conditions. These experiments harness the powerful experimental conceit of measuring extracellular phenazine reduction by *Psuedomonas* as a measureable reporter of metabolic rate, as discussed and illustrated in the preceding section and in Fig. 3.7. Specifically, we could directly and precisely measure the metabolic rate of anaerobic cells in a big set of environmental conditions using a parallel set of electrodes compatible with 96 well culture plates, as discussed and deployed recently by Ciemniecki and coworkers [5]. As theorists, we are deeply galvanized by these experimental settings and measurements. Enlightenment about how cells work, if it is to come, will be grounded in probing the high-dimensional landscape of cellular physiology by testing many different environmental modulations and their effects in calibrated, real units. Refuting, ratifying, or ultimately building candidates for emergent quantitative simplicities in microbial life can be greatly catalyzed by strains under genetic control; environments under biochemical and atmospheric control; and high-resolution measurements resolving their interplay, capabilities the work by the Newman lab advances.

In a set of pilot experiments, *P. aueriginosa* cells were provided plenty of carbon; no oxygen; three concentrations of extracellular phenazine to act as the terminal electron acceptor; and four different levels of sodium chloride, all in physiologically relevant concentration ranges. These cells were nurtured in standard MOPS minimal medium, as described previously [5, 18, 17].

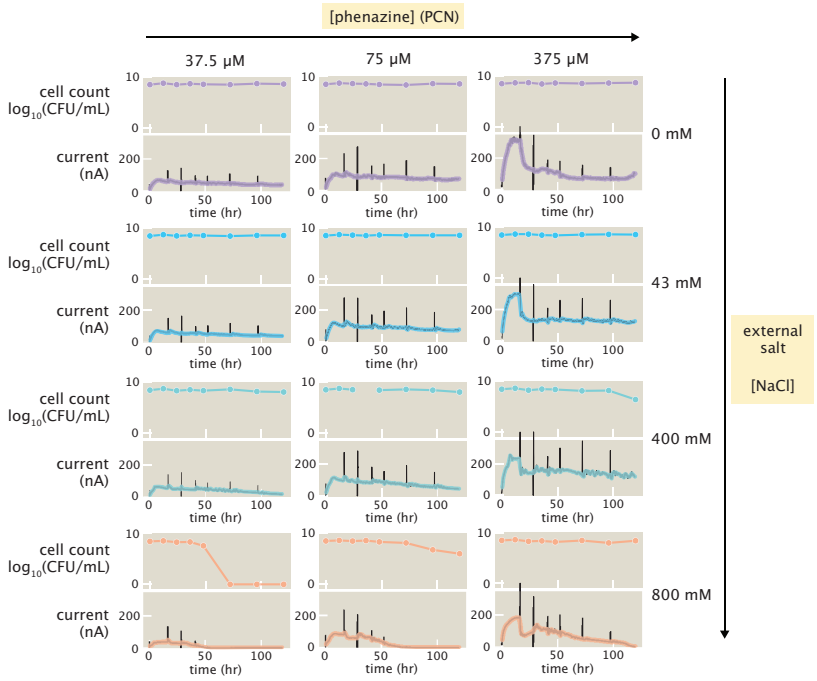

Figure 3.13: Impact of salt and external phenazine concentration on cellular abundance and current over time. The (i, j)th subplot in this grid shows the viable cell count (top axis) and total current (bottom axis) measured for the ith external sodium chloride concentration and the jth extracellular phenazine concentration condition. (In these current plots, the thin black trajectories show the raw current signal over time, including the presence of large transient spikes when very small volumes were withdrawn for purposes of counting viable cell abundance. To filter out these spikes as artifacts of measurement, we computed the median of current over one hour increments, shown as thick colored lines.)

As shown in the top axes of each plot in Figure 3.13, the bulk survival of such energetically and ionically challenged *Pseudomonas* over time varies richly with both external salt and phenazine. Specifically, more than eighty percent of cells largely survived over 120 hours and longer if they were supplied with any of the tested 37.5 μM, 75 μM, and 375 μM concentrations of phenazine and less than 400 mM of sodium chloride. However, at the substantial concentration of 800 mM sodium chloride (shown as orange traces in the bottom row of Fig. 3.13), cells with only 37.5 μM phenazine largely died between 48 hours and 72 hours; more phenazine at 75 μM enabled longer survival, and 375 μM phenazine mostly protected the cells from much death for up to 120 hours.

Accompanying these trajectories in cell abundance, the total currents sustained by these populations of cells also vary systematically as shown in the lower axes of each plot in Fig. 3.13. These trajectories in metabolic rate are also visualized by regarding these data on a per-cell basis, with per-capita metabolic rates shown in Fig. 3.14. Some general trends are manifest. Especially during the initial transient increases of measured current at early times (e.g. up to ∼twelve hours) under some conditions, larger levels of phenazine tend to manifest larger currents (as reflected by the rightmost column of Fig. 3.13). Clearly, more salt slows how quickly cells rev up their metabolic activity in the first twelve hours under the high (375 μM) phenazine condition, hinting at an evidently but curiously antagonistic relationship between phenazine and ionic context for cells as they initially strive to acclimatize (see the rightmost column of Fig. 3.14). However, the general impact of different salt concentrations is much more context- and even time- dependent, a theme we now discuss.

As shown by the surface plots in Fig. 3.15 and the full complement of two-dimensional slices in Fig. 3.16 and Fig. 3.17, the geometry of the relationship the metabolic rate per-capita to external salt and phenazine concentration changes in slope, directionality, and monotonicity over time. For instance, between zero and twelve hours (Fig. 3.15(A)

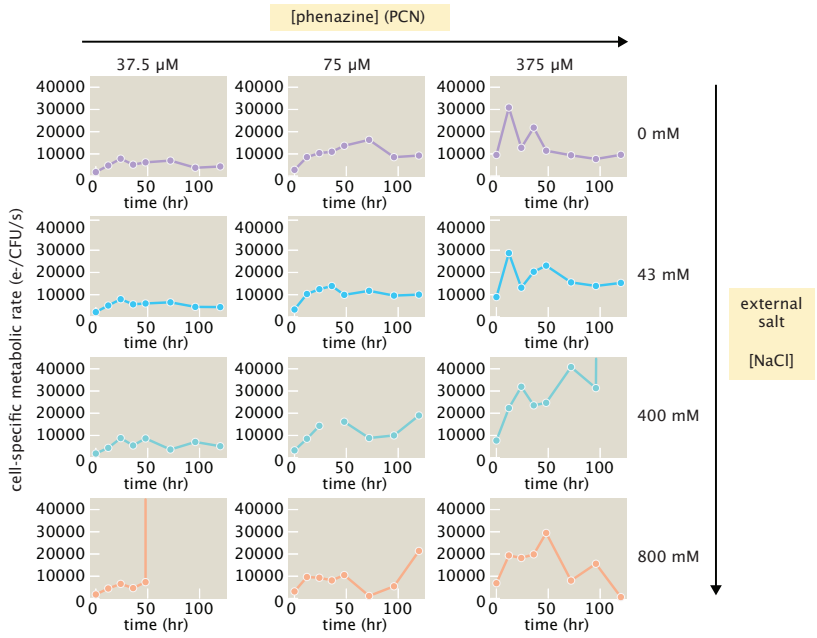

Figure 3.14: Impact of salt and external phenazine concentration on per-cell metabolic rate over time. These are are the same data as shown earlier in Figure 3.13, but visualized as a ratio to give a current per-cell. As discussed earlier in Reference [5], a current of one electron per second per cell corresponds to approximately the energy equivalent of 1 ATP hydrolysis's worth of energy per second per cell. (Here, in calculating the scale of the y-axis of metabolic rate per cell, we took the working volume of wells that cells were grown in to be 150 μL, as previously described [5]. Note that very rapid increases in per-cell metabolic rate are probably attributable to crashes in population and should be regarded as subject to the accompanying uncertainty.)

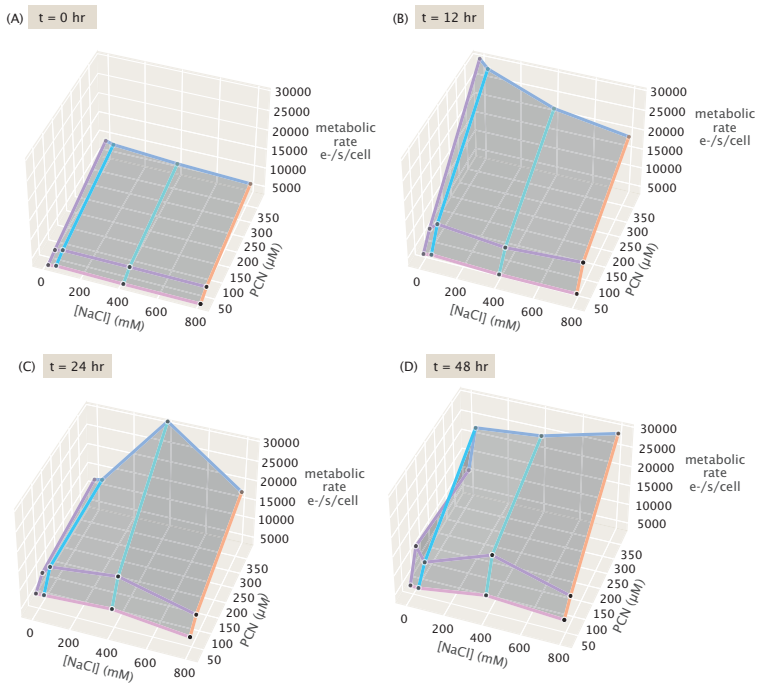

Figure 3.15: The relationships between metabolic rate per cell to phenazine and sodium chloride changes over time. (A)-(D) Metabolic rate measurements as a function of the three phenazine and four sodium chloride concentrations at timepoints $t = 0, 12, 24$, and 48 hr.

versus Fig. 3.15(B)), metabolic rate increases its steepness of variation with respect to both salt and phenazine. At intermediate times (e.g. at 24 hours), these relationships even develop peaks—for instance, metabolic rate gains a local maximum at the intermediate value of 400 mM sodium chloride, reproducible across the three phenazine concentrations (see the locally-maximal measurements connected by the light blue line in Fig. 3.15(C)). We speculate that since ions can affect or challenge virtually all aspects of cellular biochemistry, and 800 mM of external salt is a considerable ionic insult, the fact that metabolic rates can often be slower or saturating at this salt concentration may be connected to retarding a number of separate metabolically-demanding activities than those specifically associated with ion pumping. However, adjudicating such speculation demands much deeper measurements and experiments.

Many of the physiological surfaces of Figs. 3.15-3.17 insinuate cross-talk between

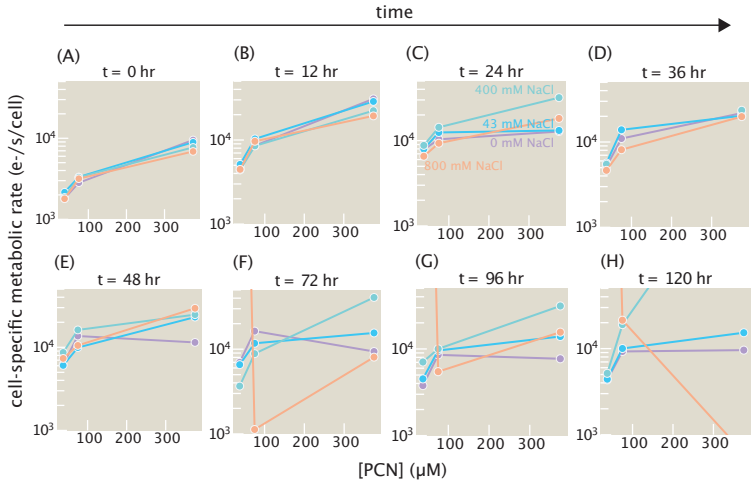

Figure 3.16: Metabolic rate per cell versus external phenazine concentrations, at increasing sodium chloride levels (indicated by purple, blue, teal, and orange lines, respectively), over time. (Note that at late times (72 hr and later), some populations have died to very small abundances, giving some frantically-varying curves to be regarded with appropriate uncertainty.)

cellular responses to external salt and external phenazine. For instance, whereas metabolic rate looks to mildly increase then gently saturate with salt concentration for low (37.5 μM and 75 μM) concentrations of phenazine, the 375 μM phenazine condition shows a continuous *decrease* in metabolic rate with external salt, as is conspicuous in the zero-hour and twelve-hour timepoints shown in Fig. 3.15(A-B) or Fig. 3.17(A-B). We hazard the tentative speculation that such interrelationships could be tied to the fact that some efflux pumps and transporters involved in exchanging toxins between the cell and the environment are coupled to sodium ions as well [19]; thus, if phenazine must be exported by the cell when its ambient concentration becomes harmful, sodium ion homeostasis may operate differently. We propose that these speculations are precisely and readily testable.

At last, we return to the quantitative question posed at the beginning of our discussion and ask quantitatively how dramatically external salt changes the metabolic demand of *Pseudomonas*. Unlike the tidy linear increase of metabolic rate with salt inferred for *E. coli* by Schink [4] (discussed in the preceding chapter), the repertoire of behaviors measured of *Pseudomonas* in Fig. 3.17 are not manifestly linear in salt, and are subject to the context

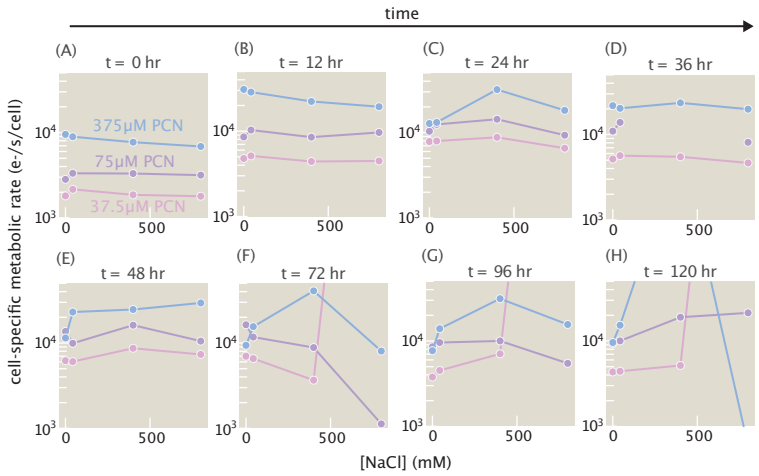

Figure 3.17: Metabolic rate per cell versus external sodium chloride concentrations, at different phenazine levels (indicated by blue, pink, and purple lines), over time. Note that at late times (72 hr and later), some populations have died to very small abundances, giving some frantically-varying curves to be regarded with appropriate uncertainty.

dependencies we just discussed. However, across these times and conditions, we see that the largest changes in metabolic rates per cell with increments of sodium chloride are much more gentle than implicated for *E. coli*. Specifically, even the instantaneous slopes of the most dramatic of these relationships are at most,

$$\kappa_{P.\ aeruginosa} \lesssim \text{few} \times 10 \text{ ATP/s/cell/(mM NaCl)}. \tag{3.41}$$

For instance, Fig. 3.18 illustrates that (for the modest perturbations of 400 mM external sodium chloride and below) and a modest level of (physiologically-well tolerated) phenazine, metabolic rate changes only of order $\kappa \lesssim 7$ ATP/s/cell/(mM NaCl). This is hugely different than *E. coli*'s number we referred to earlier ($\kappa_{E.\ coli} \sim 10^3$ ATP/s/cell/(mM NaCl)).

Two factors may contribute to the much smaller sensitivity we observed in anaerobic *Pseudomonas*'s metabolic response to salt compared to that of aerboic *E. coli*. First, these strains may themselves exhibit intrinsically different aversions to sodium ions (and

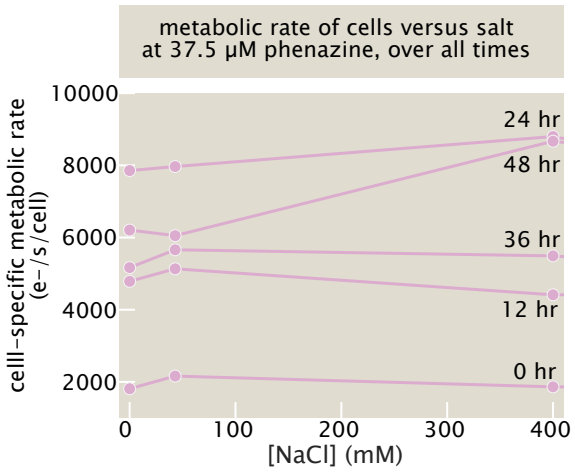

Figure 3.18: Representative subset of data, with early to intermediate timepoints ($t \leq 48$ hr) displayed, for relatively mild salt concentrations ([NaCl] $\leq$ 400 mM) for a modest, physiologically-well-tolerated phenazine concentration. Compared to the sensitivity inferred for *E. coli*, the per-cell metabolic rate for these *P. aeruginosa* clearly changes more gently over these salt ranges.

therefore pay very different pumping and other costs). Studies report that some *Pseudomonas* can allow the accumulation of cytosolic sodium to levels of order 80% of the extracellular medium in ranges of several tens of mM external sodium [20]; this apparent tolerance is in contrast to some reports on *E. coli*'s tight regulation of internal sodium concentrations [21]. If *E. coli* is intriniscally more halophobic than *Pseudomonas*, it may pay more to maintain ion homeostasis when the environment demands it. Second, the presence or absence of oxygen may fundamentally change the insults delivered by salts to many aspects of the functioning cell; in particular, damage to cellular components may occur via mechanisms dependent on salt and oxygen jointly. Absent oxygen, then, the repair costs attending these processes may be required at lower rates, overall causing less metabolic burden in response to salt.

More generally, the rich physiological manifolds hinted at in this preliminary analysis beckon to be reconciled with much more extensive measurements, perturbations, and attendent theory-building.

Bibliography

[1] Tori M Hoehler and Bo Barker Jørgensen. Microbial life under extreme energy limitation. *Nature Reviews Microbiology*, 11(2):83–94, 2013.

[2] Rachel M Walker, Valeria C Sanabria, and Hyun Youk. Microbial life in slow and stopped lanes. *Trends in microbiology*, 32(7):650–662, 2024.

[3] William R Shoemaker, Stuart E Jones, Mario E Muscarella, Megan G Behringer, Brent K Lehmkuhl, and Jay T Lennon. Microbial population dynamics and evolutionary outcomes under extreme energy limitation. *Proceedings of the National Academy of Sciences*, 118(33): e2101691118, 2021.

[4] Severin Schink, Mark Polk, Edward Athaide, Avik Mukherjee, Constantin Ammar, Xili Liu, Seungeun Oh, Yu-Fang Chang, and Markus Basan. Survival dynamics of starving bacteria are determined by ion homeostasis that maintains plasmolysis. *Nature Physics*, 20(8):1332–1338, 2024.

[5] John A Ciemniecki, Chia-Lun Ho, Richard D Horak, Akihiro Okamoto, and Dianne K Newman. Mechanistic study of a low-power bacterial maintenance state using high-throughput electrochemistry. *Cell*, 187(24):6882–6895, 2024.

[6] Severin J Schink, Elena Biselli, Constantin Ammar, and Ulrich Gerland. Death rate of *E. coli* during starvation is set by maintenance cost and biomass recycling. *Cell systems*, 9(1):64–73, 2019.

[7] Elena Biselli, Severin Josef Schink, and Ulrich Gerland. Slower growth of *Escherichia coli* leads to longer survival in carbon starvation due to a decrease in the maintenance rate. *Molecular systems biology*, 16(6):e9478, 2020.

[8] Rolf Sander. Compilation of Henry's law constants (version 5.0. 0) for water as solvent. *Atmospheric Chemistry & Physics*, 23(19), 2023.

[9] Elise S Cowley, Sebastian H Kopf, Alejandro LaRiviere, Wiebke Ziebis, and Dianne K Newman. Pediatric cystic fibrosis sputum can be chemically dynamic, anoxic, and extremely reduced due to hydrogen sulfide formation. *MBio*, 6(4):e00767–15, 2015.

[10] Rudolf K Thauer, Anne-Kristin Kaster, Henning Seedorf, Wolfgang Buckel, and Reiner Hedderich. Methanogenic archaea: ecologically relevant differences in energy conservation. *Nature Reviews Microbiology*, 6(8):579–591, 2008.

[11] Kai Schuchmann and Volker Müller. Autotrophy at the thermodynamic limit of life: a model for energy conservation in acetogenic bacteria. *Nature Reviews Microbiology*, 12(12):809–821, 2014.

[12] Georg Fuchs. CO_2 fixation in acetogenic bacteria: variations on a theme. *FEMS Microbiology Reviews*, 2(3):181–213, 1986.

[13] Alexander J Krause, Graham A Shields, Robert J Newton, and Benjamin JW Mills. Modelling sulfate concentrations in the global ocean through phanerozoic time. *Journal of the Geological Society*, 181(4):jgs2023–184, 2024.

[14] JK Böhlke, GE Ericksen, and K Revesz. Stable isotope evidence for an atmospheric origin of desert nitrate deposits in northern Chile and southern California, USA. *Chemical Geology*, 136 (1-2):135–152, 1997.

[15] Wenping Cui, Robert Marsland III, and Pankaj Mehta. Diverse communities behave like typical random ecosystems. *Physical Review E*, 104(3):034416, 2021.

[16] Yun Wang, Suzanne E Kern, and Dianne K Newman. Endogenous phenazine antibiotics promote anaerobic survival of *Pseudomonas aeruginosa* via extracellular electron transfer. *Journal of bacteriology*, 192(1):365–369, 2010.

[17] Nathaniel R Glasser, Suzanne E Kern, and Dianne K Newman. Phenazine redox cycling enhances anaerobic survival in *Pseudomonas aeruginosa* by facilitating generation of atp and a proton-motive force. *Molecular microbiology*, 92(2):399–412, 2014.

[18] Alexa Price-Whelan, Lars EP Dietrich, and Dianne K Newman. Pyocyanin alters redox homeostasis and carbon flux through central metabolic pathways in *Pseudomonas aeruginosa* pa14. *Journal of bacteriology*, 189(17):6372–6381, 2007.

[19] Wakano Ogawa, Yusuke Minato, Hayata Dodan, Motoyasu Onishi, Tomofusa Tsuchiya, and Teruo Kuroda. Characterization of mate-type multidrug efflux pumps from *Klebsiella pneumoniae* mgh78578. *PloS one*, 10(3):e0121619, 2015.

[20] Tibor I Matula and Robert A Macleod. Penetration of *Pseudomonas aeruginosa* by sodium chloride and its relation to the mechanism of optical effects. *Journal of Bacteriology*, 100(1): 411–416, 1969.

[21] Chien-Jung Lo, Mark C Leake, and Richard M Berry. Fluorescence measurement of intracellular sodium concentration in single *Escherichia coli* cells. *Biophysical journal*, 90(1):357–365, 2006.